Hepatology Research 2008; 38: 886–895 doi: 10.1111/j.1872-034X.2008.00324.x

Original Article

Activation of B-Myb by E2F1 in hepatocellular carcinoma

Tomoaki Nakajima,[1] Kohichiroh Yasui,[1] Keika Zen,[1] Yoshikazu Inagaki,[1] Hideki Fujii,[1] Masahito Minami,[1] Shinji Tanaka,[2] Masafumi Taniwaki,[3] Yoshito Itoh,[1] Shigeki Arii,[2] Johji Inazawa[4] and Takeshi Okanoue[1]

[1]Molecular Gastroenterology and Hepatology, [3]Molecular Hematology and Oncology, Graduate School of Medical Science, Kyoto Prefectural University of Medicine, Kyoto, [2]Department of Hepato-Biliary-Pancreatic Surgery, and [4]Department of Molecular Cytogenetics, Medical Research Institute, Tokyo Medical and Dental University, Tokyo, Japan

Aim: Deregulation of E2F1 transcriptional activity is observed in a variety of cancers, including hepatocellular carcinoma (HCC). The aim of the present study is to identify transcriptional target genes of E2F1 in HCC.

Methods: We determined expression levels for *E2F1* and ten candidate genes thought to be targets of E2F1 in primary HCCs using a real-time quantitative reverse transcription-PCR assay. Following small interfering RNA (siRNA)-mediated knockdown of *E2F1* in HCC cell lines, we quantified mRNA levels of the candidate E2F1 target genes.

Results: *E2F1* was significantly over-expressed in 41 primary HCCs as compared to non-tumorous liver tissues. Among the candidates, *MYBL2*, whose product is the transcriptional factor B-Myb, which is involved in controlling cell-cycle progression and apoptosis, was significantly over-expressed in primary HCCs. Additionally, expression levels of *MYBL2* correlated with those of *E2F1*. Knockdown of *E2F1* resulted in a decrease in expression of *MYBL2*. A copy-number gain for *MYBL2* was observed in 36 of 66 primary HCCs, suggesting that *MYBL2* expression is up-regulated by amplification in addition to being regulated by E2F1. Moreover, siRNA-mediated knockdown of *MYBL2* led to reduced expression of *CDC2* (which encodes CDC2), cyclin A2 (*CCNA2*), and topoisomerase II α (*TOP2A*), implicating these genes in the cell cycle and suggesting that they may be downstream targets of B-Myb.

Conclusion: *MYBL2* is a probable transcriptional target of E2F1 in HCC and may therefore be a useful biomarker for diagnosis and an attractive target for molecular therapies useful to treat HCC.

Key words: CCNA2, CDC2, E2F1, hepatocellular carcinoma, MYBL2, TOP2A

INTRODUCTION

HEPATOCELLULAR CARCINOMA (HCC) is the fifth most common malignancy in the world and is estimated to result in approximately half a million deaths annually.[1] Several risk factors for HCC have been reported, including infection with hepatitis B virus (HBV), hepatitis C virus (HCV), dietary aflatoxin, alcohol consumption, and diabetes.

Deregulation of E2F transcriptional activity as a result of alterations in the $p16^{INK4a}$-cyclin D1-Rb pathway is a hallmark of human cancer. E2Fs comprise a family of related factors that control the expression of genes important for cell-cycle progression as well as other processes such as apoptosis, DNA repair, and differentiation.[2,3] There are now eight known human E2F family genes: *E2F1-E2F8*. The E2F1 through to E2F6 proteins dimerize with one of three DP proteins (DP1, DP2/3, or DP4) to form functional transcriptional factor complexes that can bind DNA with high affinity. The function of the E2F-DP heterodimer is thought to be determined primarily by which E2F is present in the heterodimeric complex.

Our earlier studies identified *TFDP1*, which encodes DP1, as a probable target within a 13q34 amplicon that is frequently detected in HCCs[4] and esophageal squamous cell carcinomas.[5] Elevated expression of *TFDP1* was associated with large HCC tumor size and down-regulation of *TFDP1* inhibited growth of HCC cells.[6]

Correspondence: Dr Kohichiroh Yasui, Molecular Gastroenterology and Hepatology, Graduate School of Medical Science, Kyoto Prefectural University of Medicine, Kyoto, 465 Kajii-cho, Kamigyo-ku, Kyoto 602-8566, Japan. Email: yasuik@koto.kpu-m.ac.jp
Received 12 November 2007; revision 13 December 2007; accepted 13 December 2007.

Amplification of *E2F1* has been reported in some cancer cell lines and *E2F1* may be a target for the chromosome 20q amplification.[2] High levels of E2F1 in cancers of the lung, breast, and pancreas correlate with poor clinical outcomes.[2] In contrast, reduced E2F1 expression in colon cancer and bladder cancer correlates with more aggressive malignancy. Paradoxically, E2F1 has been shown to have the ability to induce both cell-cycle progression and programmed cell death, potentially leading to both tumor-promoting and tumor-suppressing effects.[7] Deregulation of E2F1 expression can lead to promotion or inhibition of tumorigenesis, depending on what other oncogenic mutations are present.[2]

B-Myb belongs to the Myb family of transcriptional factors, which include A-Myb and C-Myb.[8] Whereas A-Myb and C-Myb are tissue-specific, B-Myb is expressed ubiquitously. B-Myb plays an important role in the cell cycle and in cell survival.[8,9] *MYBL2*, which encodes B-Myb, is induced by E2F1.[10] B-Myb expression is barely detectable in G0 and is induced at the G1/S transition of the cell cycle.[8] The broad expression of B-Myb in proliferating cells at least in part explains the phenotype of B-Myb knockout mice; that is, death in early embryogenesis.[11]

Herein we examined *E2F1* expression in HCC and explored transcriptional targets of E2F1 that are activated in this type of tumor. Intriguingly, *MYBL2* emerged as a likely downstream target of E2F1. Further, we show that B-Myb protein can activate expression of genes that encode CDC2, cyclin A2, and topoisomerase II α, which are required for cell cycle progression.

METHODS

Cell lines and tumor samples

A TOTAL OF 21 liver cancer cell lines were examined in this study: HCC-derived HLE;[12] HLF;[12] PLC/PRF/5; Li7;[13] Huh7; Hep3B; SNU354;[14] SNU368;[14] SNU387;[14] SNU398;[14] SNU423;[14] SNU449;[14] SNU475;[14] JHH-1;[15] JHH-2;[15] JHH-4;[15] JHH-5;[15] JHH-6;[15] JHH-7;[15] Huh-1;[16] and the hepatoblastoma line HepG2. All cell lines were maintained in Dulbecco's modified Eagle's medium (DMEM) supplemented with 10% fetal bovine serum. We obtained a total of 66 primary HCC tumors from patients undergoing surgery at the Tokyo Medical and Dental University and Kyoto University. Before initiation of the present study, informed consent was obtained in the formal style approved by all relevant ethical committees. Genomic DNA was isolated from each cell line and from primary tumors using the Puregene DNA isolation kit (Gentra, MN, USA). Total RNA could be extracted from 41 of these primary HCCs.

Fluorescence *in situ* hybridization (FISH)

We performed FISH using as a probe the bacterial artificial chromosome (BAC) RP11-73E4, which includes *MYBL2*, as described previously.[4] Briefly, the probe was labeled by nick translation with biotin-16-dUTP (Roche Diagnostics, Germany) and hybridized to metaphase chromosomes. Hybridization signals for biotin-labeled probes were detected with avidin-fluorescein (Roche Diagnostics).

Real-time PCR

We quantified genomic DNA and mRNA by real-time fluorescence detection. Total RNA was obtained using Trizol (Invitrogen, CA, USA). Residual genomic DNA was removed by incubating the RNA samples with RNase-free DNase I (Takara Bio, Japan) prior to reverse transcription (RT)-PCR. Single-stranded complementary DNA (cDNA) was generated using Superscript III Reverse Transcriptase (Invitrogen) following the manufacturer's directions. Real-time quantitative PCR experiments were performed with the LightCycler system using Faststart DNA Master Plus SYBR Green I (Roche Diagnostics) according to the manufacturer's protocol. Primer sequences are listed in supplementary Tables S1 and S2. *GAPDH*[17] and long interspersed nuclear element-1 (LINE-1)[18] were used as endogenous controls for mRNA and genomic DNA levels, respectively.

RNA interference studies

For RNA interference (RNAi), small interfering RNA (siRNA) duplex oligoribonucleotides targeting *E2F1* or *MYBL2*, along with a non-silencing control siRNA which has no significant similarity to any known mammalian gene, were obtained from Qiagen (Japan). The siRNAs were delivered into JHH-5 cells using Hyperfect transfection reagent (Qiagen) according to the manufacturer's instructions. To determine mRNA levels, cells were harvested 48 h after transfection and subjected to real-time quantitative RT-PCR as described above.

Statistical analysis

All statistical analyses were performed using SPSS version 15.0 (SPSS, IL, USA). Either the Wilcoxon signed-rank test or the Mann–Whitney *U*-test was used to compare mRNA levels among tumorous and non-tumorous tissues. Any apparent associations were tested via Pearson's correlation coefficient analysis. χ^2-tests

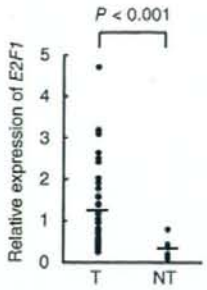

Figure 1 Over-expression of *E2F1* in primary hepatocellular carcinoma (HCC). Relative expression levels of *E2F1* in 41 primary HCC tumors (T) and seven non-tumorous liver tissues (NT) were evaluated by real-time quantitative RT-PCR and normalized to *GAPDH*. Horizontal lines indicate the means of expression levels.

were used to evaluate associations between clinicopathological parameters and the level of *MYBL2* expression. *P* values of <0.05 were considered significant.

RESULTS

Identification of E2F1 downstream genes

WE DETERMINED THE levels of *E2F1* mRNA in 41 primary HCCs and seven non-tumorous liver tissues using real-time quantitative RT-PCR. *E2F1* was significantly over-expressed in HCC tumors as compared to non-tumorous tissues (Mann–Whitney *U*-test, $P < 0.001$; Fig. 1).

To identify genes induced by E2F1 in HCC, we examined ten candidate genes thought to be targets of E2F1: *MYBL2* (which encodes B-Myb); *CDC2* (CDC2/CDK1); *CCNA2* (cyclin A2); *CCNE1* (cyclin E); *MYC* (c-MYC); *DHFR* (dihydrofolate reductase); *TYMS* (thymidylate synthetase); *TK1* (thymidine kinase 1); *RRM1* (ribonucleotide reductase M1); and *PCNA* (proliferating cell nuclear antigen). For this purpose, we knocked down expression of *E2F1* via siRNA. In HCC-derived JHH-5 cells that received siRNA targeting *E2F1*, we observed a decrease in *E2F1* mRNA levels relative to what was observed for cells that received a control siRNA or for untreated cells (Fig. 2A). Following siRNA-mediated knockdown of *E2F1*, we quantified mRNA levels of the ten candidate genes. Knockdown of *E2F1* led to a decrease in expression of *MYBL2*, *CCNE1*, *MYC*, *TK1*, and *RRM1*, but not *CDC2*, *CCNA2*, *DHFR*, *TYMS*, or *PCNA* (Fig. 2A).

We next determined the expression levels of the ten candidate genes in 41 primary HCCs and seven non-tumorous liver tissues. Real-time quantitative RT-PCR analyses revealed that *MYBL2*, *CDC2*, and *CCNA2* were significantly over-expressed in HCC tumors as compared to non-tumor tissues (Fig. 2B). Among the ten candidates, only *MYBL2* was down-regulated following siRNA-mediated knockdown of *E2F1* and significantly over-expressed in primary HCCs. Therefore, we chose to further analyze *MYBL2*, which encodes the transcriptional factor B-Myb.

To further test if over-expression of *MYBL2* correlates with primary HCC tumors, we quantified *MYBL2* expression in paired tumor and non-tumor tissues from an additional 22 patients with HCC. *MYBL2* was significantly over-expressed in 20 (91%) of the tumors as compared to their non-tumorous counterparts (Wilcoxon signed-rank test, $P < 0.001$; Fig. 2C). Further, the expression of *MYBL2* significantly correlated with those of *E2F1* in the 22 primary HCC tumors (Fig. 2D) and in the 21 HCC cell lines (Fig. 2E). Taken together, these observations indicate that *MYBL2* is up-regulated in HCC and is a probable transcriptional target of E2F1.

To clarify the relationship between expression of *MYBL2* and various clinicopathological parameters, we

Figure 2 *MYBL2* is up-regulated in hepatocellular carcinoma (HCC) and is a probable transcriptional target of *E2F1*. (A) siRNA-mediated knockdown of *E2F1* in HCC cell lines. JHH-5 cells were treated with 5 nM siRNA targeting *E2F1* (si*E2F1*) or control siRNA (non-silencing) and harvested 48 h after transfection. Untreated cells were maintained under identical experimental conditions. Relative expression of *E2F1* and its ten putative downstream genes was evaluated by real-time quantitative RT-PCR. Results are presented as the ratio between expression of each gene and a reference gene (*GAPDH*) to correct for variation in the amount of RNA. Relative expression levels were normalized such that for untreated cells, this ratio is 1. (B) Expression of ten putative *E2F1*-downstream genes in 41 primary HCC tumors (T) relative to expression in seven non-tumorous liver tissues (NT). Horizontal lines indicate the means of expression levels. (C) Relative expression of *MYBL2* in paired tumor (T) and non-tumor (NT) tissues from 22 patients with HCC. (D, E) Correlation between expression levels of *E2F1* and *MYBL2* in 22 primary HCC tumors (D) and 21 HCC cell lines (E). Pearson's correlation coefficient analysis revealed that there was a significant correlation between expression levels of the two genes. (□) untreated, (▨) non-silencing, (■) siE2F1.

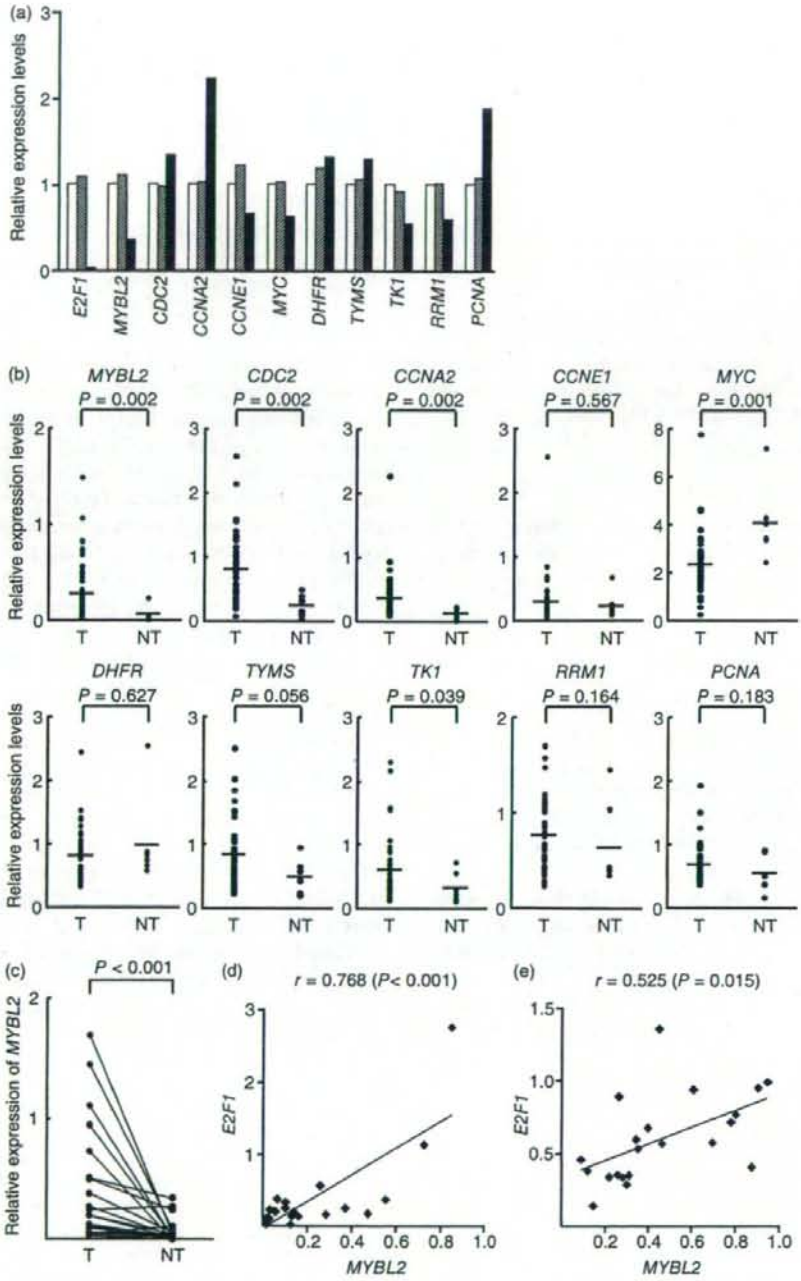

Table 1 Relationship between clinicopathological features and expression levels of *MYBL2* in 37 hepatocellular carcinomas (HCC)

	MYBL2		*P**
	Low (≤ median) ($n = 19$)	High (> median) ($n = 18$)	
Age			
<65	6	13	0.013
≥65	13	5	
Sex			
Male	13	14	0.522
Female	6	4	
Tumor size			
<5 cm	8	11	0.248
≥5 cm	11	7	
Tumor differentiation			
Well	3	2	0.403
Moderate	11	14	
Poorly	5	2	
Stage			
I, II, III	16	12	0.214
IV	3	6	
HBV infection status			
Positive	2	6	0.158
Negative	16	10	
Unknown	1	2	
HCV infection status			
Positive	15	11	0.491
Negative	3	5	
Unknown	1	2	
Backgroud liver tissue			
Normal	1	1	0.492
Chronic hepatitis	15	11	
Liver Cirrhosis	1	4	
Unknown	2	2	

*χ^2 test.

next examined the available data from 37 HCC patients, whose tumors were divided into high- and low-expression groups based on where they fell relative to the median of level of *MYBL2* mRNA expression (Table 1). High expression of *MYBL2* was significantly associated with samples from patients less than 65 years old as compared with samples from patients 65 and older. However, we observed no significant link with any other parameter that was examined, including the sex of the patient, the size, degree of differentiation, or stage of the tumor, HBV or HCV infection, or features of non-tumorous liver samples from these patients.

Amplification of *MYBL2* in HCC

Amplification of chromosomal DNA is one of several mechanisms capable of activating genes, a phenomenon that contributes to the development and progression of cancers. *MYBL2* is located at 20q13, where a gain in DNA copy number is frequently observed in various tumors,[19] including HCC.[20] Based on this observation, we decided to determine the *MYBL2* copy number in DNA derived from 21 liver cancer cell lines (20 HCC cells and the hepatoblastoma line HepG2) using real-time quantitative PCR. Copy number changes were counted as gains if the results for a given cell line exceeded the mean plus twice the standard deviation of the levels of *MYBL2* observed in genomic DNA derived from four samples of peripheral blood lymphocytes (i.e. from normal cells). *MYBL2* exhibited copy-number gain in 19 of the 20 lines (Fig. 3A). We then used FISH to more directly test copy-number gain of *MYBL2* in these cell lines. In JHH-5 cells, a representative example, the number of FISH signals was higher than normal (i.e. seven signals were detected in single cells; Fig. 3B). In addition, to ask if *MYBL2* was amplified in primary tumors, we examined 66 primary HCCs for a gain in copy number. Copy-number gain for *MYBL2* was observed in 36 of the 66 tumors (55%; Fig. 3C). These findings suggested that copy-number gain of *MYBL2* acts synergistically with transcriptional activity of E2F1 to upregulate *MYBL2* expression in HCCs.

B-Myb downstream genes

To explore B-Myb-inducible genes in HCC, we analyzed eight genes previously reported to be downstream targets of B-Myb: *CDC2*;[21] *CCNA2*;[22] *TOP2A* (which encodes DNA topoisomerase II α);[23] *FGF4* (fibroblast growth factor 4);[24] *POLA* (DNA polymerase α);[25] *CCND1* (cyclin D1);[21] *CLU* (clusterin/ApoJ);[26] and *BCL2* (BCL-2).[27] Of these, *CDC2*, *CCNA2*, *TOP2A*, *FGF4*, *POLA*, and *CCND1* have been implicated in progression of cell cycle, and *CLU* and *BCL2* appear to be involved in anti-apoptotic activity. We knocked down expression of *MYBL2* via siRNA in JHH-5 cells (Fig. 4A). Upon siRNA-mediated knockdown of *MYBL2*, we observed reduced expression of only *CDC2*, *CCNA2*, and *TOP2A* among the eight candidate genes examined (Fig. 4A). These three genes (*CDC2*, *CCNA2*, and *TOP2A*) were significantly over-expressed in 22 primary HCC tumors as compared with their counterpart non-tumorous tissues (Fig. 4B); that is, *CDC2* was over-expressed in 21 HCC tumors (95%); *CCNA2* in 20 (91%); and *TOP2A* in 19 (86%). Moreover, expression levels of *MYBL2*

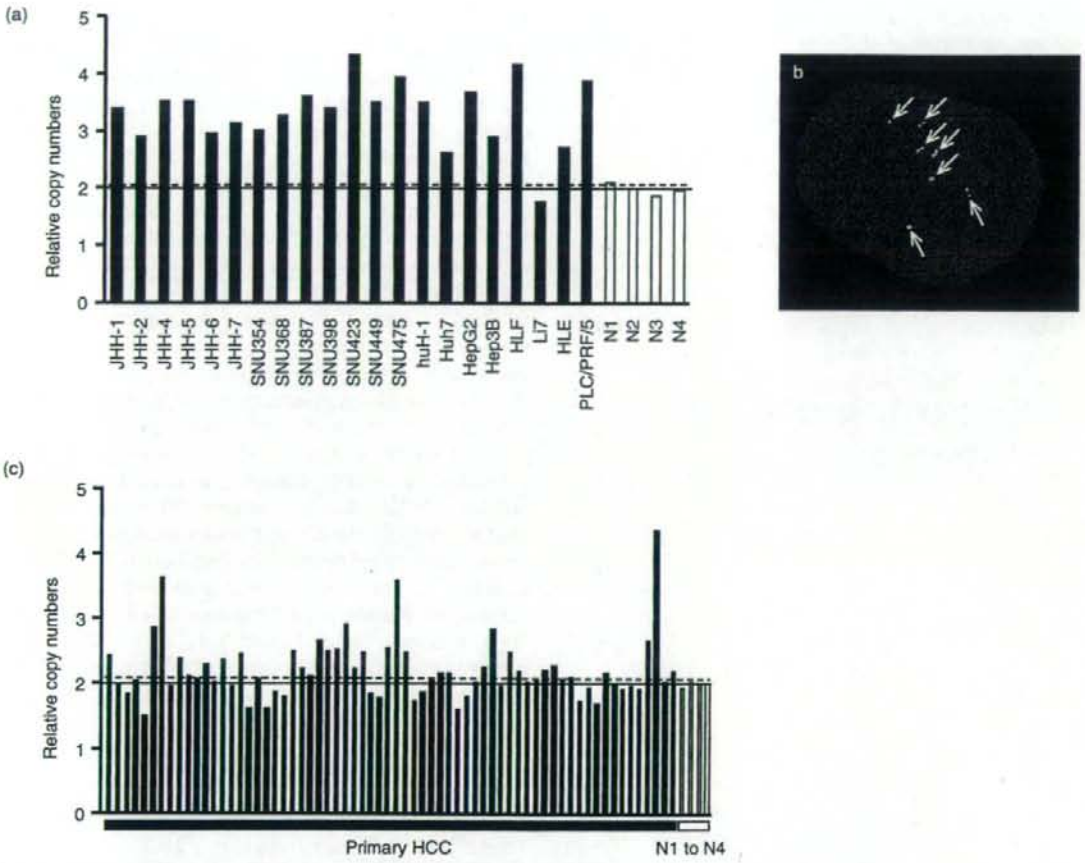

Figure 3 Amplification of *MYBL2* in hepatocellular carcinoma (HCC). (A) Relative copy number of *MYBL2* determined by real-time quantitative PCR in 21 HCC cell lines and normal peripheral lymphocytes (N1 to N4). Results are presented as the ratio between *MYBL2* and a LINE-1 control, and were normalized such that the average ratio in four normal DNAs (N1 to N4) is 2 (solid horizontal line). The mean + 2 × SD of normal lymphocytes (dotted line) was used as the cut-off for a copy-number gain. (B) Representative image of interphase FISH for *MYBL2* in JHH-5 cells. In this case, seven twin-spot FISH signals can be observed. (C) Relative copy number of *MYBL2* in 66 primary HCC tumors determined as in (A). Values were normalized such that the average copy number of *MYBL2* in genomic DNA derived from four normal lymphocytes is 2 (solid horizontal line). The mean + 2 × SD of normal lymphocytes (dotted line) was used as the cut-off for a copy-number gain.

significantly correlated with those of *CDC2*, *CCNA2*, and *TOP2A* in 22 primary HCCs (Fig. 4C). These results suggest that *CDC2*, *CCNA2*, and *TOP2A* are probable transcriptional targets of B-Myb in HCC.

DISCUSSION

IN THE PRESENT study, we examined expression of *E2F1* and candidate E2F1 target genes in primary HCCs. Our results show that both *E2F1* and *MYBL2* are over-expressed in primary HCCs (Figs 1,2B,C) and that there is a significant correlation between expression of *E2F1* and *MYBL2* (Fig. 2D). RNAi-mediated reduction of *E2F1* in HCC-derived cells inhibits expression of *MYBL2* (Fig. 2A). These findings suggest that *MYBL2* may be a transcriptional target of E2F1, which could explain the upregulation of *MYBL2* we observed in HCC. Furthermore, a gain in *MYBL2* copy-number was frequently observed in both HCC cell lines and primary HCC tumors (Fig. 3). Thus, in addition to

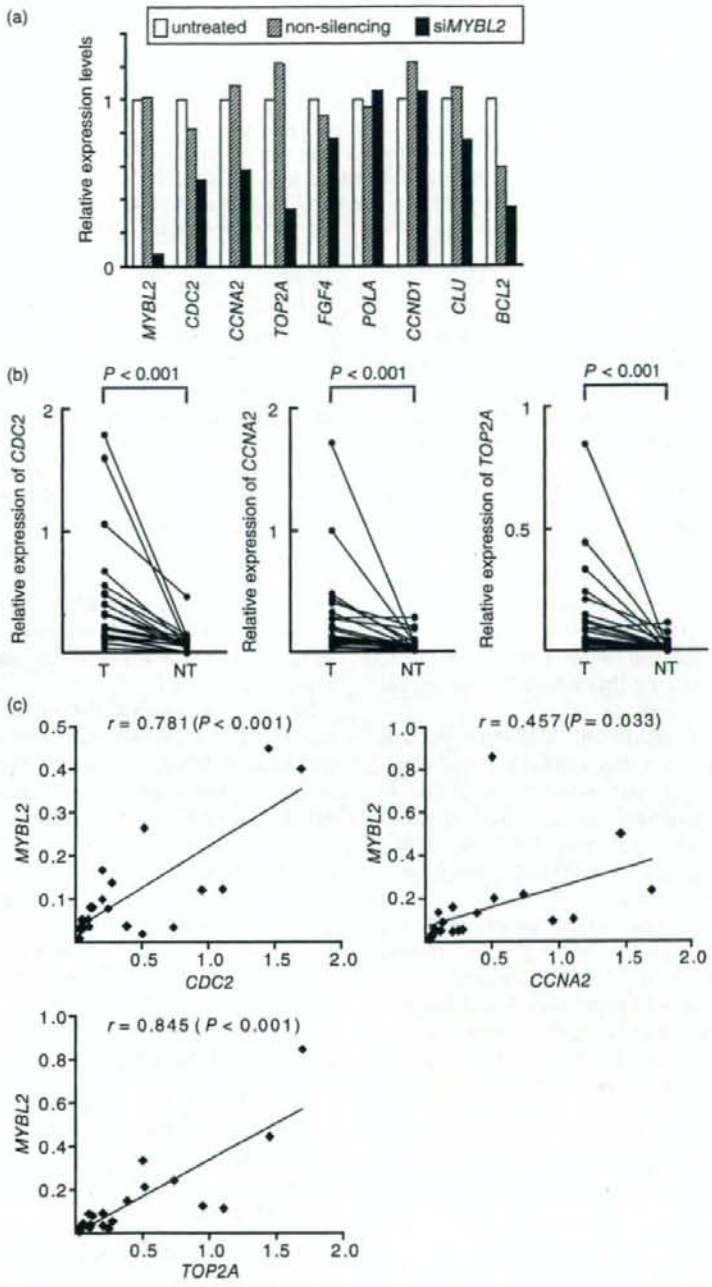

Figure 4 *CDC2*, *CCNA2*, and *TOP2A* are probable transcriptional targets of *MYBL2* in hepatocellular carcinoma (HCC). (A) siRNA-mediated knockdown of *MYBL2* in HCC cell lines. JHH-5 cells were treated with 5 nM siRNA targeting *MYBL2* (si*MYBL2*) or control siRNA (non-silencing), and harvested 48 h after transfection. Untreated cells were maintained under identical experimental conditions. Relative expression of *MYBL2* and putative downstream genes were evaluated by real-time quantitative RT-PCR. Results are presented as the ratio between expression of each gene and a reference (*GAPDH*) to correct for variation in the amount of RNA. Relative expression levels were normalized such that the ratio in untreated cells is 1. (B) Relative expression of *CDC2*, *CCNA2*, and *TOP2A* in paired tumor (T) and non-tumor (NT) tissues from 22 patients as determined by real-time quantitative RT-PCR. (C) Correlation between expression of *MYBL2* and that of *CDC2*, *CCNA2*, or *TOP2A* in 22 primary HCC tumors. Pearson's correlation coefficient analysis revealed that there was a significant correlation between the level of expression of *MYBL2* and that of each of the three genes.

transcriptional activation of *MYBL2* by E2F1, expression of *MYBL2* may also be upregulated in HCC as a result of amplification of the *MYBL2*-containin genomic region in these cells.

Our results are consistent with earlier research. *MYBL2* is frequently amplified in a variety of tumor types, including breast,[28] ovarian,[29] melanoma,[30] and HCC.[31] Moreover, *MYBL2* is amplified and over-expressed in breast cancer cell lines.[32] *MYBL2* is over-expressed in prostate metastases relative to localized tumors.[33] Elevated expression of *MYBL2* is also observed in advanced neuroblastoma and correlates with a poor prognosis.[34] Although the direct role of B-Myb in cancers is not yet fully established, these lines of evidence, together with ours, indicate that B-Myb has oncogenic potential.

We also looked at the relationship between expression levels of *MYBL2* in primary HCCs and clinicopathological parameters (Table 1). With the exception of the age of the patient, no parameter tested, including tumor size, differentiation or stage, correlated with *MYBL2* expression. This may suggest that *MYBL2* is upregulated in early stages of HCC formation.

We next examined transcriptional targets of B-Myb in HCC. Among the eight candidate genes examined, only *CDC2*, *CCNA2*, and *TOP2A* were suppressed at the mRNA level following siRNA-mediated knockdown of *MYBL2* (Fig. 4A). Correspondingly, these three genes are significantly over-expressed in primary HCC tumors (Fig. 4B) and expression of the three genes correlates with *MYBL2* expression (Fig. 4C). These results suggest that *CDC2*, *CCNA2*, and *TOP2A* are downstream targets of B-Myb. Interestingly, Cyclin A2, which is encoded by *CCNA2*, forms a complex with CDC2, whose activity peaks at the G2/M transition of cell cycle, and CDC2-cyclin A2 kinase activity is required to enter M phase. Our results are consistent with the recent findings that B-Myb, together with E2F1, regulates expression of genes required for the G2/M phase of the cell cycle, such as CDC2, cyclin A2, and cyclin B1.[22]

We found that si-RNA-mediated reduction of *E2F1* inhibited expression of *MYBL2*, but not *CCNA2* (Fig. 2A). However, si-RNA-mediated knockdown of *MYBL2* inhibited expression of *CCNA2* (Fig. 4A). It is unclear why reduction of *E2F1* did not lead to a decrease in expression of *CCNA2* through a decrease in the expression of *MYBL2*. There might be a time lag between suppression of *MYBL2* and *CCNA2* expression following si-RNA-mediated knockdown of *E2F1*.

Topoisomerase II α, which is encoded by *TOP2A*, forms breaks in double-stranded DNA, allowing strands to separate during replication. Cyclin A2, CDC2, and topoisomerase II α are all essential for cell cycle progression. Thus, these genes seem reasonable target for B-Myb regulation.

We have shown that *E2F1* is over-expressed in primary HCC tumors and that *MYBL2* expression is also up-regulated in HCCs, suggesting that *MYBL2* is a transcriptional target of E2F1. Frequent amplification of *MYBL2* in HCCs is likely to be an additional mechanism leading to *MYBL2* over-expression. Further, the *CDC2*, *CCNA2*, and *TOP2A* genes may be transcriptional targets of B-Myb. Our results suggest that B-Myb may play an important role in initiation or progression (or both) of HCC and thus, may represent an optimal target for development of novel therapies for this widespread tumor type.

ACKNOWLEDGMENT

THIS WORK WAS supported by Grants-in-Aid for Scientific Research from the Japan Society for the Program of Science (KY).

REFERENCES

1 El-serag HB. Hepatocellular carcinoma: an epidemiologic view. *J Clin Gastroenterol* 2002; 35: S72–8.
2 Johnson DG, Degregori J. Putting the oncogenic and tumor suppressive activities of E2F into context. *Curr Mol Med* 2006; 6: 731–8.

3 DeGregori J, Johnson DG. Distinct and overlapping roles for E2F family members in transcription. proliferation and apoptosis. *Curr Mol Med* 2006; 6: 739–48.
4 Yasui K, Arii S, Zhao C *et al.* TFDP1, CUL4A, and CDC16 identified as targets for amplification at 13q34 in hepatocellular carcinomas. *Hepatology* 2002; 35: 1476–84.
5 Shinomiya T, Mori T, Ariyama Y *et al.* Comparative genomic hybridization of squamous cell carcinoma of the esophagus: the possible involvement of the DP1 gene in the 13q34 amplicon. *Genes Chromosomes Cancer* 1999; 24: 337–44.
6 Yasui K, Okamoto H, Arii S, Inazawa J. Association of over-expressed TFDP1 with progression of hepatocellular carcinomas. *J Hum Genet* 2003; 48: 609–13.
7 Bell LA, Ryan KM. Life and death decisions by E2F-1. *Cell Death Differ* 2004; 11: 137–42.
8 Sala A. B-MY B, a transcription factor implicated in regulating cell cycle, apoptosis and cancer. *Eur J Cancer* 2005; 41: 2479–84.
9 Joaquin M, Watson RJ. Cell cycle regulation by the B-Myb transcription factor. *Cell Mol Life Sci* 2003; 60: 2389–401.
10 DeGregori J, Kowalik T, Nevins JR. Cellular targets for activation by the E2F1 transcription factor include DNA synthesis- and G1/S-regulatory genes. *Mol Cell Biol* 1995; 15: 4215–24.
11 Tanaka Y, Patestos NP, Maekawa T, Ishii S. B-myb is required for inner cell mass formation at an early stage of development. *J Biol Chem* 1999; 274: 28067–70.
12 Dor I, Namba M, Sato J. Establishment and some biological characteristics of human hepatoma cell lines. *Gann* 1975; 66: 385–92.
13 Hirohashi S, Shimosato Y, Kameya T *et al.* Production of alpha-fetoprotein and normal serum proteins by xenotransplanted human hepatomas in relation to their growth and morphology. *Cancer Res* 1979; 39: 1819–28.
14 Park JG, Lee JH, Kang MS *et al.* Characterization of cell lines established from human hepatocellular carcinoma. *Int J Cancer* 1995; 62: 276–82.
15 Fujise K, Nagamori S, Hasumura S *et al.* Integration of hepatitis B virus DNA into cells of six established human hepatocellular carcinoma cell lines. *Hepatogastroenterology* 1990; 37: 457–60.
16 Huh N, Utakoji T. Production of HBs-antigen by two new human hepatoma cell lines and its enhancement by dexamethasone. *Gann* 1981; 72: 178–9.
17 Minamiya Y, Matsuzaki I, Sageshima M *et al.* Expression of tissue factor mRNA and invasion of blood vessels by tumor cells in non-small cell lung cancer. *Surg Today* 2004; 34: 1–5.
18 Zhao X, Li C, Paez JG *et al.* An integrated view of copy number and allelic alterations in the cancer genome using single nucleotide polymorphism arrays. *Cancer Res* 2004; 64: 3060–71.
19 Knuutila S, Björkqvist AM, Autio K *et al.* DNA copy number amplifications in human neoplasms: review of comparative genomic hybridization studies. *Am J Pathol* 2000; 157: 689.
20 Okamoto H, Yasui K, Zhao C, Arii S, Inazawa J. PTK2 and EIF3S3 genes may be amplification targets at 8q23-q24 and are associated with large hepatocellular carcinomas. *Hepatology* 2003; 38: 1242–9.
21 Sala A, Calabretta B. Regulation of BALB/c 3T3 fibroblast proliferation by B-myb is accompanied by selective activation of cdc2 and cyclin D1 expression. *Proc Natl Acad Sci USA* 1992; 89: 10415–19.
22 Zhu W, Giangrande PH, Nevins JR. E2Fs link the control of G1/S and G2/M transcription. *EMBO J* 2004; 23: 4615–26.
23 Brandt TL, Fraser DJ, Leal S, Halandras PM, Kroll AR, Kroll DJ. c-Myb trans-activates the human DNA topoisomerase II alpha gene promoter. *J Biol Chem* 1997; 272: 6278–84.
24 Johnson LR, Johnson TK, Desler M *et al.* Effects of B-Myb on gene transcription: phosphorylation-dependent activity ans acetylation by p300. *J Biol Chem* 2002; 277: 4088–97.
25 Watson RJ, Robinson C, Lam EW. Transcription regulation by murine B-myb is distinct from that by c-myb. *Nucleic Acids Res* 1993; 21: 267–72.
26 Cervellera M, Raschella G, Santilli G *et al.* Direct transactivation of the anti-apoptotic gene apolipoprotein J (clusterin) by B-MYB. *J Biol Chem* 2000; 275: 21055–60.
27 Grassilli E, Salomoni P, Perrotti D, Franceschi C, Calabretta B. Resistance to apoptosis in CTLL-2 cells overexpressing B-Myb is associated with B-Myb-dependent bcl-2 induction. *Cancer Res* 1999; 59: 2451–6.
28 Ginestier C, Cervera N, Finetti P *et al.* Prognosis and gene expression profiling of 20q13-amplified breast cancers. *Clin Cancer Res* 2006; 12: 4533–44.
29 Tanner MM, Grenman S, Koul A *et al.* Frequent amplification of chromosomal region 20q12-q13 in ovarian cancer. *Clin Cancer Res* 2000; 6: 1833–9.
30 Koynova DK, Jordanova ES, Milev AD *et al.* Gene-specific fluorescence in-situ hybridization analysis on tissue microarray to refine the region of chromosome 20q amplification in melanoma. *Melanoma Res* 2007; 17: 37–41.
31 Zondervan PE, Wink J, Alers JC *et al.* Molecular cytogenetic evaluation of virus-associated and non-viral hepatocellular carcinoma: analysis of 26 carcinomas and 12 concurrent dysplasias. *J Pathol* 2000; 192: 207–15.
32 Forozan F, Mahlamäki EH, Monni O *et al.* Comparative genomic hybridization analysis of 38 breast cancer cell lines: a basis for interpreting complementary DNA microarray data. *Cancer Res* 2000; 60: 4519–25.
33 Bar-Shira A, Pinthus JH, Rozovsky U *et al.* Multiple genes in human 20q13 chromosomal region are involved in an advanced prostate cancer xenograft. *Cancer Res* 2002; 62: 6803–7.

34 Raschellà G, Cesi V, Amendola R *et al.* Expression of B-myb in neuroblastoma tumors is a poor prognostic factor independent from MYCN amplification. *Cancer Res* 1999; 59: 3365–8.

SUPPLEMENTARY MATERIAL

THE FOLLOWING SUPPLEMENTARY material is available for this article online:

Table S1. Primer sequences used for RT-PCR assays.

Table S2. Primer sequences used for genomic PCR assays.

This material is available as part of the online article from http://www.blackwell-synergy.com

ELSEVIER

Cancer Genetics and Cytogenetics 180 (2008) 30–36

CANCER GENETICS AND CYTOGENETICS

CREB3L4, *INTS3*, and *SNAPAP* are targets for the 1q21 amplicon frequently detected in hepatocellular carcinoma

Yoshikazu Inagaki[a], Kohichiroh Yasui[a,*], Mio Endo[a], Tomoaki Nakajima[a], Keika Zen[a], Kazuhiro Tsuji[a], Masahito Minami[a], Shinji Tanaka[b], Masafumi Taniwaki[c], Yoshito Itoh[a], Shigeki Arii[b], Takeshi Okanoue[a]

[a]*Molecular Gastroenterology and Hepatology, Graduate School of Medical Science, Kyoto Prefectural University of Medicine, 465 Kajii-cho Kamigyo-ku, Kyoto 602-8566, Japan*

[b]*Department of Hepato-Biliary-Pancreatic Surgery, Tokyo Medical and Dental University, Tokyo, Japan*

[c]*Molecular Hematology and Oncology, Graduate School of Medical Science, Kyoto Prefectural University of Medicine, Kyoto, Japan*

Received 10 August 2007; accepted 25 September 2007

Abstract High-density single nucleotide polymorphism (SNP) array analysis revealed novel amplification at 1q21 in cell lines derived from hepatocellular carcinomas (HCCs). Fluorescence in situ hybridization and real-time quantitative polymerase chain reaction studies verified amplification at 1q21. An increase in copy number at the region was detected in 32 of the 36 primary HCC tumors (89%). To identify the targets for amplification, we examined 19 HCC cell lines for expression levels of all 26 genes located within the 700-kb amplified region. Five genes were overexpressed in cell lines with amplification at 1q21. Among these, *CREB3L4* (cAMP responsive element binding protein 3-like 4), *INTS3* (integrator complex subunit 3), and *SNAPAP* (SNAP-associated protein) were significantly overexpressed in tumors from 18 HCC patients, compared with counterpart nontumorous tissues. The findings suggest that *CREB3L4*, *INTS3*, and *SNAPAP* are probable targets for the amplification mechanism and may therefore be involved, together or separately, in the development or progression of HCCs.

1. Introduction

Amplification of DNA in certain chromosome regions plays a crucial role in the development and progression of human malignancies, specifically when proto-oncogenic target genes within those amplicons are overexpressed. Oncogenes that are often amplified in cancers include *MYC*, *ERBB2*, and *CCND1*. The initial approach to genome-wide detection of copy number aberrations in cancers was comparative genomic hybridization (CGH) [1]. Using CGH analyses, we detected novel regions of amplification in various types of tumor. Within these amplicons, we identified a number of additional proto-oncogenes that may be upregulated by DNA amplification [2–6]. CGH has limited resolution (5–10 Mb), however, in that it detects segmental copy number changes on metaphase chromosomes [1].

The recent introduction of high-density oligonucleotide microarrays designed for typing of single nucleotide polymorphisms (SNPs) allows for high-resolution mapping of chromosomal amplifications, deletions, and loss of heterozygosity [7–11]. The GeneChip Mapping 100K array set (Affymetrix, Santa Clara, CA) contains 116,204 SNP loci, with a mean intermarker distance of 23.6 kb, and enables detailed and genome-wide identification of DNA copy number changes [12–14].

In the present study, we identified novel, high-level amplification at 1q21 using the Affymetrix GeneChip Mapping 100K array analysis against a panel of cell lines derived from hepatocellular carcinoma (HCC). Worldwide, HCC is the fifth most common malignancy in men and the eighth most common in women [15]. Previous CGH studies of HCC, including ours [3], have revealed that the most frequent copy number gains occur on 1q (58–78%) [16–18]. Gains in 1q21~q23 were identified as a genomic event associated with the early development of HCC [19]. Recurrent gains at 1q21~q23 have been observed in not only HCC but also in tumors including squamous cell carcinomas of the head and neck, lung cancer, desmoid tumors, and sarcomas [20,21]. These findings suggest that 1q21 harbors one or more proto-oncogenes whose overexpression following amplification contributes to the initiation or

* Corresponding author. Tel.: +81-75-251-5519; fax: +81-75-251-0710.

E-mail address: yasuik@koto.kpu-m.ac.jp (K. Yasui).

0165-4608/08/$ – see front matter
doi:10.1016/j.cancergencyto.2007.09.013

progression of HCC. We therefore performed molecular definition of the 1q21 amplicon. Three genes emerged as possible targets: *CREB3L4*, *INTS3*, and *SNAPAP*.

2. Materials and methods

2.1. Cell lines and tumor samples

A total of 19 HCC-derived cell lines were examined: HLE [22], HLF [22], PLC/PRF/5 [23], Li7 [24], Huh7 [25], Hep3B [26], SNU354 [27], SNU368 [27], SNU387 [27], SNU398 [27], SNU423 [27], SNU475 [27], JHH-1 [28], JHH-2 [28], JHH-4 [28], JHH-5 [28], JHH-6 [28], JHH-7 [28], and Huh-1 [29]. All cell lines were maintained in Dulbecco's modified Eagle's medium (DMEM) supplemented with 10% fetal bovine serum. We obtained 36 primary HCC tumors from patients undergoing surgery at the hospital of Tokyo Medical and Dental University and Kyoto University. Genomic DNA was isolated from all cell lines and primary tumors using the Puregene DNA isolation kit (Gentra Systems, Minneapolis, MN).

Informed consent and Ethics Committee approval were obtained before initiation of the study.

2.2. SNP assay

GeneChip Mapping 100K array set (Affymetrix, Santa Clara, CA) analyses were performed according to the manufacturer's instructions. Briefly, 250 ng of genomic DNA was digested with a restriction enzyme (*Xba*I or *Hin*dIII), ligated to an adaptor, and amplified by polymerase chain reaction (PCR) [8,9,30]. Amplified products were fragmented, labeled by biotinylation, and hybridized to microarrays. Hybridization was detected by incubation with streptavidin–phycoerythrin conjugate, followed by scanning, and analysis was performed as described previously [30,31].

Copy number changes were calculated based on SNP hybridization signal intensity data from the experimental sample relative to intensity distributions derived from a reference set containing > 100 individuals using the Affymetrix Chromosome Copy Number Analysis Tool software and algorithm (CNAT version 2.0; http://www.affymetrix.com/support/developer/tools/affytools.affy) [32].

2.3. Real-time quantitative PCR

We quantified genomic DNA and mRNA using the real-time fluorescence detection method. Total RNA was obtained using Trizol reagent (Invitrogen, Carlsbad, CA). Residual genomic DNA was removed by incubating RNA samples with RNase-free DNase I (Takara Bio, Shiga, Japan) prior to reverse transcriptase PCR. Single-stranded complementary DNA (cDNA) was generated using SuperScript III reverse transcriptase (Invitrogen) according to the manufacturer's directions. Real-time quantitative PCR

Table 1
Primer sequences used for real-time quantitative polymerase chain reaction (PCR)

Gene	Forward primer	Reverse primer	PCR product size, bp
S100A6	5′-GAAGGAGCTGAAGGAGCTGA-3′	5′-CCCTTGAGGGCTTCATTGTA-3′	177
S100A5	5′-AGAGCTGTGTCTIGGGGAGA-3′	5′-CCCTGGTCACTTGTTGTCCT-3′	166
S100A4	5′-GATGAGCAACTTGGACAGCA-3′	5′-CTICCTGGGCTGCTTATCTG-3′	127
S100A3	5′-CGAGGTGGACTTTGTGGAGT-3′	5′-GGGCCTCCTAGGTAAAATGG-3′	244
S100A2	5′-CTTCCTGGGTCTGTCTCTGC-3′	5′-TCCCCCTTACTCAGCTTGAA-3′	142
S100A16	5′-ATGTTCCTGCCAAATTCCTG-3′	5′-GAGAGGTCTCTGCTGCTGCT-3′	142
S10014	5′-CTGACCCCTTCTGAGCTACG-3′	5′-CCAGAGGGAGTTCTCAGTGC-3′	214
S100A13	5′-TCCAACTGGAACCTIGAACC-3′	5′-GATCTGGAAGTGGGTGGAGA-3′	155
S100A1	5′-GGAGACCCTCATCAACGTGT-3′	5′-CAGCCACAAGCACCACATAC-3′	215
C1orf77	5′-GGTGGTAGAGGTCGGGGTAT-3′	5′-GCATCCAGGTGTCCTITTGT-3′	167
SNAPAP	5′-AGGAACGACTGAGACGGCTA-3′	5′-GTAAATTCCCGAATCCAGCA-3′	80
ILF2	5′-CGTGGAAAGCCTAAGAGCAC-3′	5′-GAAGATTGGGTGGCACTGTT-3′	128
NPR1	5′-GCATTGAGCTGACACGAAAA-3′	5′-CCTTGACGATGTCATTGGTG-3′	219
INTS3	5′-GGTACGGGAACTGGTGAAGA-3′	5′-CTGCTCTTCAGGACCCACTC-3′	162
SLC27A3	5′-ATACCTGGGAGCGTTTTGTG-3′	5′-CCGCTGTCCTGTGTAGTTGA-3′	104
GATAD2B	5′-TICTTTGCCCTCTGTGCTTT-3′	5′-GGCATCTCGTACCTCTGAGC-3′	221
KIAA0476[a]	5′-CTATGGGCTGTGGTICCTGT-3′	5′-TGCCCATAGTGTGAGCAGAG-3′	171
CRTC2	5′-TICAGTGCAGTCCTCAGGTG-3′	5′-GCTGAACTGCTCCAGATTCC-3′	145
SLC39A1	5′-GGATIGGGGAAGACACTTGA-3′	5′-GAAATGGGCTAGGACCAACA-3′	159
CREB3L4	5′-GACCAGAAGCTGGGTCTGAG-3′	5′-TGTTACGTCCTTGTGGGTCA-3′	77
JTB	5′-ACGTATTGTCCCTGCTCACC-3′	5′-GCTGCTCACTGGGAATTAGC-3′	165
RAB13	5′-GAGCCATGGGCATIATCCTA-3′	5′-CCTTCTGCACCTTCCTCTTG-3′	162
RPS27	5′-CGCAAAGGATCTCCTTCATC-3′	5′-CGTTTGTGCATGGCTAAAGA-3′	148
NUP210L	5′-CTGTGAACAGAGGGCTGACA-3′	5′-GCTCAATGGCATGCTCTACA-3′	96
TPM3	5′-GGGTTTGAAGCTGCTGTCTC-3′	5′-CCACAAACCCAAAGCAAAGT-3′	137
C1orf89	5′-ATGCAGGACACCATGGTACA-3′	5′-TCCTGCTGGTACTGCTGATG-3′	113

[a] The approved gene symbol for the *KIAA0476* gene is now *DENND4B* (http://www.genenames.org). For simplicity, the previous symbol is retained.

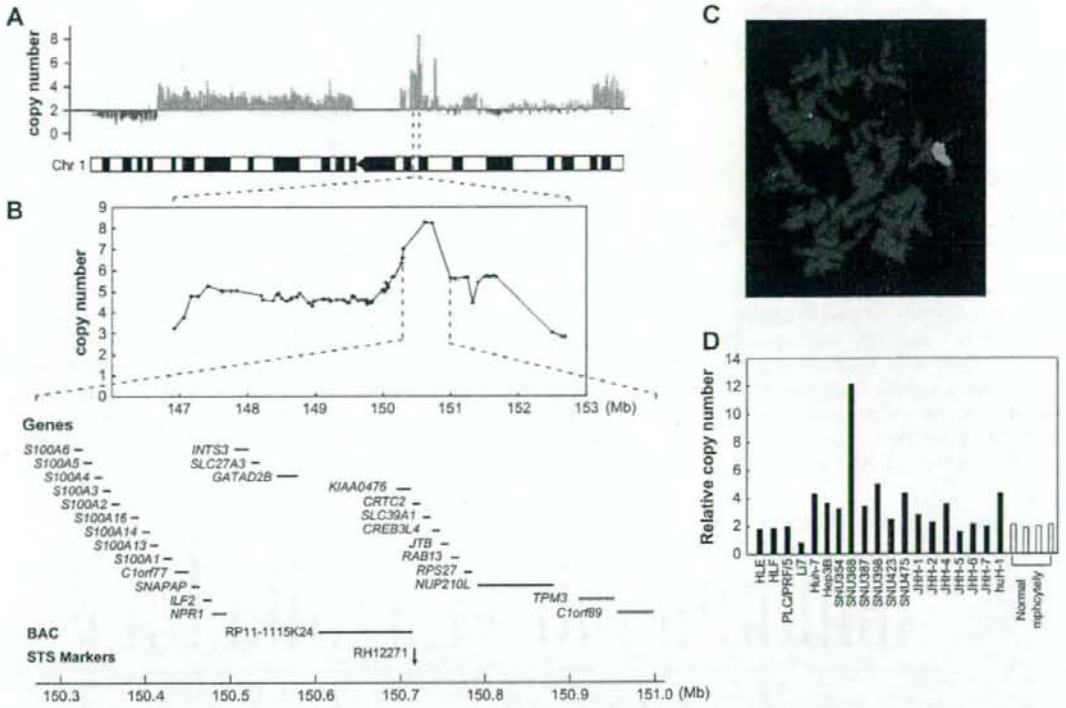

Fig. 1. Map of the amplicon at 1q21 in the hepatocellular carcinoma (HCC) cell line SNU368. (A) Copy number determined by SNP 100 K arrays (upper) and chromosome 1 cytoband map (lower) are shown. Copy number values were estimated using the Affymetrix CNAT chromosome copy number analysis tool. Green lines show copy number gains; red lines correspond to losses of genomic material. (B) Map of 1q21 amplicon. The graph represents the copy number determined by SNP arrays. The positions of the 26 genes within the amplicon, the bacterial artificial chromosome (BAC; RP11-1115K24) used as a probe for fluorescence in situ hybridization (FISH), and the STS marker (RH12271) used for real-time quantitative polymerase chain reaction (PCR) are shown, according to the UCSC genome database (http://genome.ucsc.edu/). (C) Representative FISH images using BAC RP11-1115K24 on metaphase chromosomes from SNU368 cells. The image shows strong homogeneously staining region signals on a marker chromosome. (D) Copy numbers at the STS marker locus RH12271 in 19 HCC cell lines and four normal peripheral blood lymphocytes, as measured by real-time quantitative PCR with reference to LINE-1 controls. Values are normalized such that the average copy number in genomic DNA derived from four normal lymphocytes has a value of 2.

experiments were performed with the LightCycler system using FastStart DNA Master Plus SYBR Green I (Roche Diagnostics, Penzberg, Germany) according to the manufacturer's protocol. Primers used for PCR (listed in Table 1) were designed using Primer3 version 0.4 (http://frodo.wi.mit.edu/cgi-bin/primer3/primer3_www.cgi) on the basis of sequence data obtained from the U.S. National Center for Biotechnology Information Entrez Gene database (http://www.ncbi.nlm.nih.gov/). GAPDH [33] and long interspersed nuclear element 1 (LINE-1) [9] were used as endogenous controls for mRNA and genomic DNA levels, respectively.

2.4. Fluorescence in situ hybridization

Fluorescence in situ hybridization (FISH) experiments were performed using bacterial artificial chromosome (BAC; RP11-1115K24) as a probe, as described previously [2]. Briefly, the probe was labeled with biotin-16-dUTP

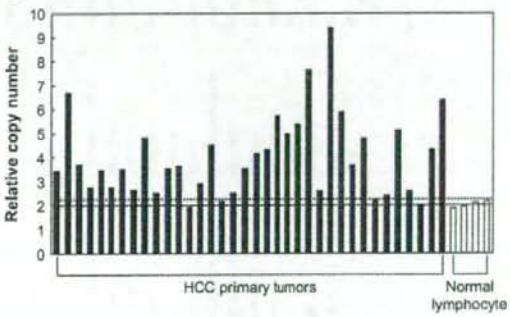

Fig. 2. Copy number gain at 1q21 in primary HCC tumors. Copy number at the STS marker locus RH12271 in 36 primary HCC tumors and four normal peripheral blood lymphocytes were determined by real-time quantitative PCR with reference to LINE-1 controls. Values are normalized such that the average copy number in genomic DNA derived from four normal lymphocytes has a value of 2 (solid horizontal line). The mean + 2 × SD of normal lymphocytes was used to determine the cutoff value for copy number gain (dotted horizontal line).

(Roche Diagnostics) by nick translation and was hybridized to metaphase chromosomes. Hybridization signals for biotin-labeled probes were detected using avidin–fluorescein (Roche Diagnostics).

3. Results

3.1. Detection of 1q21 amplicon in HCC cell lines by SNP array analysis

In the course of investigating DNA copy number aberrations in HCC cell lines by high-density SNP microarray (Affymetrix GeneChip Mapping 100K array), we found that SNU368 cells exhibited high-level amplification at 1q21 (Figs. 1A, 1B). The extent of this amplicon was estimated to be 700 kb (between Affymetrix SNP_A-1737869 and SNP_A-1662365). FISH analysis in SNU368 cells, using BAC RP11-1115K24 as a probe (Fig. 1B), revealed a strong homogeneously staining region (HSR), indicating high-level amplification (Fig. 1C). Furthermore, we determined gene dosage at the STS marker RH12271 (Fig. 1B) locus present within the amplicon by real-time quantitative PCR using DNA derived from 19 HCC cell lines. Amplification at the locus was observed in SNU368 cells (Fig. 1D). These findings confirmed amplification at 1q21 in SNU368 cells.

3.2. Amplification of 1q21 locus in primary HCC tumors

To determine whether the 1q21 region was amplified in primary tumors, we examined copy numbers at STS marker RH12271 in 36 primary HCCs by real-time quantitative PCR. Copy number changes were rated as gains if they exceeded the mean plus 2 standard deviations of the levels in normal genomic DNA derived from four peripheral blood lymphocytes. The locus was amplified in 32 of the 36 tumors (89%) (Fig. 2).

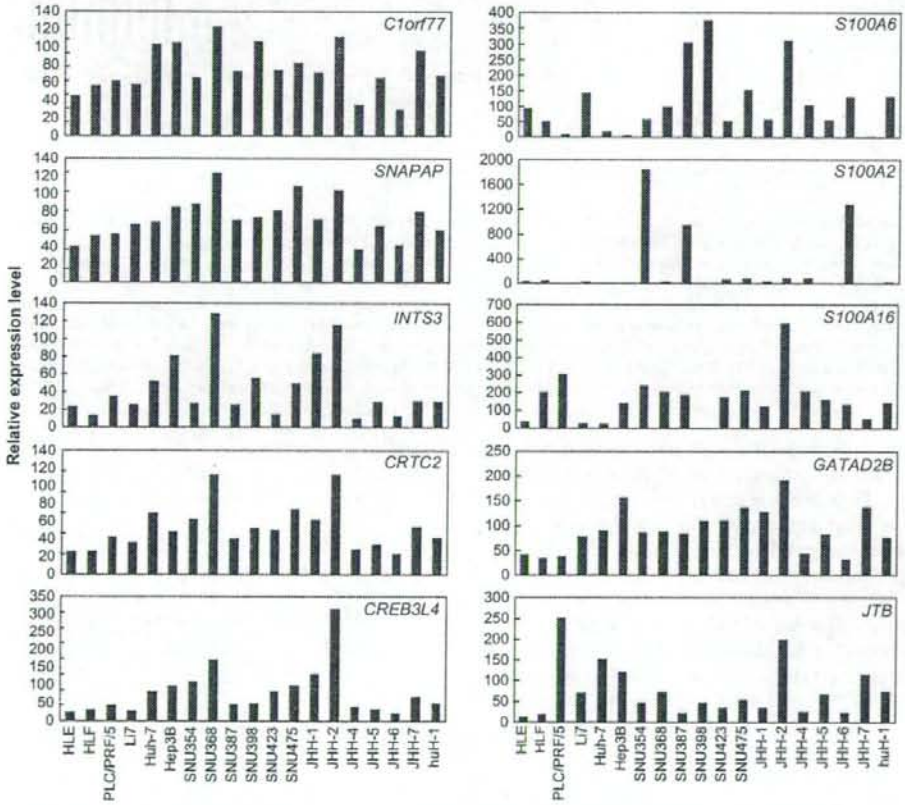

Fig. 3. Relative expression levels of 10 representative genes within the 1q21 amplicon in our panel of 19 HCC cell lines, as evaluated by real-time quantitative reverse transcriptase PCR. Results are presented as expression levels of each gene relative to a reference gene (*GAPDH*) to correct for variations in the amount of RNA. Five of the 10 genes (left: *C1orf77*, *SNAPAP*, *INTS3*, *CRTC2*, and *CREB3L4*) were overexpressed in SNU368 cells; the other 5 genes were not overexpressed (right: *S100A6*, *S100A2*, *S100A16*, *GATAD2B*, and *JTB*).

3.3. Identification of candidate target genes in 1q21 amplicon

To explore candidate target genes involved in 1q21 amplification, we determined the expression levels of all 26 genes within the amplicon in our panel of 19 HCC cell lines by real-time quantitative reverse transcriptase PCR. Five genes (*C1orf77*, *SNAPAP*, *INTS3*, *CRTC2*, and *CREB3L4*) were found to be overexpressed in SNU368 cells showing amplification at 1q21, as shown in Figure 3. In several other lines, one or more of those five genes was overexpressed without amplification. These findings suggested that the five genes are candidate targets for 1q21 amplification.

3.4. Upregulated expression of CREB3L4, INTS3, and SNAPAP in primary HCC tumors

We determined the expression levels of the five candidate genes in paired tumor and nontumor tissues from 18 HCC patients using real-time quantitative reverse transcriptase PCR. *CREB3L4*, *INTS3*, and *SNAPAP* were significantly overexpressed in 14 (78%), 14 (78%), and 13 (72%) of the tumors, respectively, compared with their counterpart nontumorous tissues (Wilcoxon signed-rank test; $P = 0.006$, $P = 0.015$, and $P = 0.014$, respectively) (Fig. 4). On the other hand, expression of *C1orf77* or *CRTC2* was not upregulated in HCC tumors. These results suggest that *CREB3L4*, *INTS3*, and *SNAPAP* are probable target for the 1q21 amplicon.

4. Discussion

The high-density SNP array analysis successfully identified high-level amplification in the narrow region at 1q21 in HCC cell lines (Figs. 1A, 1B). Frequent amplification in this region has been observed not only in HCC cell lines but also in primary HCC tumors (Figs. 1D, 2). Possible oncogenes such as *ETV3* (alias *PE-1*) [34], *MUC1* [35], and *NTRK1* (alias *TRK*) [36] are located within 1q21. Three growth-related genes located in 1q21, *HAX1*, *SHC1*, and *CKS1B*, were shown to be upregulated in HCC tumors, compared with the nontumorous tissues [37]; however, the positions of these genes were outside the amplicon we detected. The results of subsequent experiments suggest that *CREB3L4*, *INTS3*, and *SNAPAP* are probable targets for the amplicon among the 26 genes examined; the three transcripts were overexpressed in SNU368 cells that exhibited amplification (Fig. 3) and were significantly upregulated in primary HCC tumors, compared with their nontumorous counterparts (Fig. 4).

CREB3L4 (cyclic AMP responsive element binding protein 3-like 4), also referred to as AIbZIP [38], belongs to the CREB/ATF family of transcriptional factors. In humans, CREB3L4 transcripts are detected exclusively in the prostate, as well as in prostate and breast cancer cell lines [38]. Immunostaining of prostate tumors showed that CREB3L4 protein levels were higher in cancerous prostate cells than in adjacent noncancerous cells [38]. *INTS3*

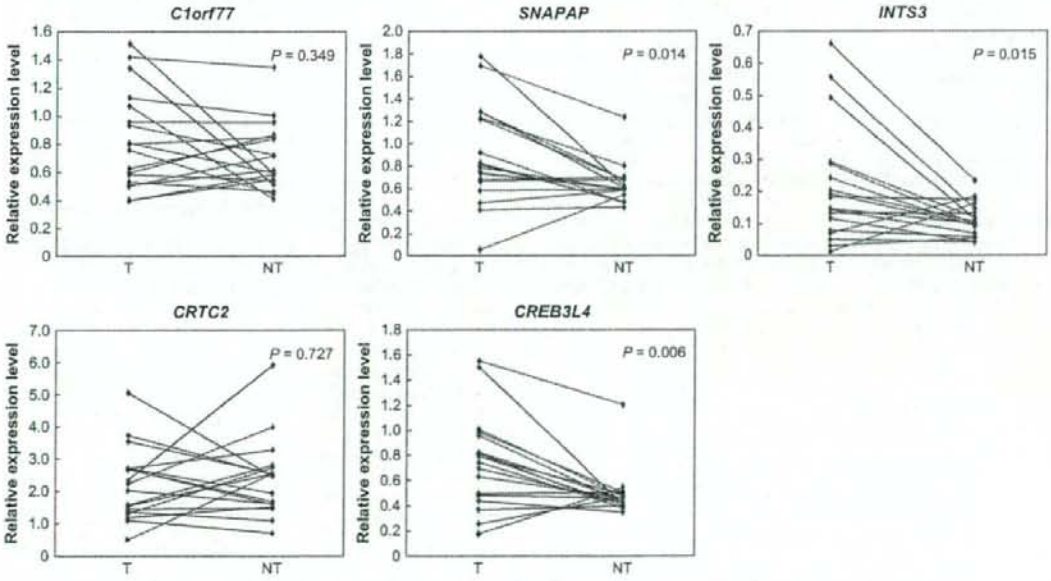

Fig. 4. Relative expression of *C1orf77*, *SNAPAP*, *INTS3*, *CRTC2*, and *CREB3L4* in paired tumor (T) and nontumor tissues (NT) from 18 patients with primary HCC. *CREB3L4*, *INTS3*, and *SNAPAP* were significantly overexpressed in primary HCC tumors. Expression levels of each gene were evaluated by real-time quantitative reverse transcriptase PCR and normalized against levels of *GAPDH*.

(integrator complex subunit 3) encodes one of the subunits of the Integrator complex. Baillat et al. [39] described an RNA polymerase II complex that contains at least 12 novel subunits, termed the Integrator, in addition to core RNA polymerase II subunits. The Integrator is found to be associated with the C-terminal domain of RNA polymerase II and mediates the processing of small nuclear RNAs (snRNAs). SNAPAP (snare-associated protein; also known as Snapin), is a component of the SNARE complex of proteins that is implicated in synaptic vesicle docking and fusion [40], and is also a component of biogenesis of lysosome-related organelles complex-1 (BLOC-1), a ubiquitously expressed multisubunit protein complex required for the normal biogenesis of specialized organelles of the endosomal-lysosomal system [41]. Little is known about the possible relationships between *INTS3* or *SNAPAP* and tumorigenesis.

Functional studies are needed to clarify the roles of these three genes in 1q21 amplification, because it is possible that coactivation of these genes leads to development and progression not only of HCCs but also of other types of tumors.

Acknowledgments

This work was supported by Grants-in-Aid for Scientific Research from the Japan Society for the Program of Science to K.Y. and T.O.

References

[1] Kallioniemi A, Kallioniemi OP, Sudar D, Rutovitz D, Gray JW, Waldman F, Pinkel D. Comparative genomic hybridization for molecular cytogenetic analysis of solid tumors. Science 1992;258:818–21.

[2] Yasui K, Arii S, Zhao C, Imoto I, Ueda M, Nagai H, Emi M, Inazawa J. TFDP1, CUL4A, and CDC16 identified as targets for amplification at 13q34 in hepatocellular carcinomas. Hepatology 2002; 35:1476–84.

[3] Okamoto H, Yasui K, Zhao C, Arii S, Inazawa J. *PTK2* and *EIF3S3* genes may be amplification targets at 8q23-q24 and are associated with large hepatocellular carcinomas. Hepatology 2003;38:1242–9.

[4] Fukuda Y, Kurihara N, Imoto I, Yasui K, Yoshida M, Yanagihara K, Park JG, Nakamura Y, Inazawa J. *CD44* is a potential target of amplification within the 11p13 amplicon detected in gastric cancer cell lines. Genes Chromosomes Cancer 2000;29:315–24.

[5] Yokoi S, Yasui K, Saito-Ohara F, Koshikawa K, Iizasa T, Fujisawa T, Terasaki T, Horii A, Takahashi T, Hirohashi S, Inazawa J. A novel target gene, *SKP2*, within the 5p13 amplicon that is frequently detected in small cell lung cancers. Am J Pathol 2002;161:207–16.

[6] Yokoi S, Yasui K, Iizasa T, Imoto I, Fujisawa T, Inazawa J. *TERC* identified as a probable target within the 3q26 amplicon that is detected frequently in non-small cell lung cancers. Clin Cancer Res 2003;9:4705–13.

[7] Mei R, Galipeau PC, Prass C, Berno A, Ghandour G, Patil N, Wolff RK, Chee MS, Reid BJ, Lockhart DJ. Genome-wide detection of allelic imbalance using human SNPs and high-density DNA arrays. Genome Res 2000;10:1126–37.

[8] Matsuzaki H, Loi H, Dong S, Tsai YY, Fang J, Law J, Di X, Liu WM, Yang G, Liu G, Huang J, Kennedy GC, Ryder TB, Marcus GA, Walsh PS, Shriver MD, Puck JM, Jones KW, Mei R. Parallel genotyping of over 10,000 SNPs using a one-primer assay on a high-density oligonucleotide array. Genome Res 2004;14:414–25. [Erratum in: Genome Res 2004;14:786].

[9] Zhao X, Li C, Paez JG, Chin K, Janne PA, Chen TH, Girard L, Minna J, Christiani D, Leo C, Gray JW, Sellers WR, Meyerson M. An integrated view of copy number and allelic alterations in the cancer genome using single nucleotide polymorphism arrays. Cancer Res 2004;64:3060–71.

[10] Bignell GR, Huang J, Greshock J, Watt S, Butler A, West S, Grigorova M, Jones KW, Wei W, Stratton MR, Futreal PA, Weber B, Shapero MH, Wooster R. High-resolution analysis of DNA copy number using oligonucleotide microarrays. Genome Res 2004;14:287–95.

[11] Wong KK, Tsang YT, Shen J, Cheng RS, Chang YM, Man TK, Lau CC. Allelic imbalance analysis by high-density single-nucleotide polymorphic allele (SNP) array with whole genome amplified DNA. Nucleic Acids Res 2004;32:e69.

[12] Matsuzaki H, Dong S, Loi H, Di X, Liu G, Hubbell E, Law J, Berntsen T, Chadha M, Hui H, Yang G, Kennedy GC, Webster TA, Cawley S, Walsh PS, Jones KW, Fodor SP, Mei R. Genotyping over 100,000 SNPs on a pair of oligonucleotide arrays. Nat Methods 2004;1:109–11.

[13] Garraway LA, Widlund HR, Rubin MA, Getz G. Integrative genomic analyses identify *MITF* as a lineage survival oncogene amplified in malignant melanoma. Nature 2005;436:117–22.

[14] Zhao X, Weir BA, LaFramboise T, Lin M, Beroukhim R, Garraway L, Beheshti J, Lee JC, Naoki K, Richards WG, Sugarbaker D, Chen F, Rubin MA, Jänne PA, Girard L, Minna J, Christiani D, Li C, Sellers WR, Meyerson M. Homozygous deletions and chromosome amplifications in human lung carcinomas revealed by single nucleotide polymorphism array analysis. Cancer Res 2005;65:5561–70.

[15] Bosch FX, Ribes J, Cléries R, Díaz M. Epidemiology of hepatocellular carcinoma. Clin Liver Dis 2005;9:191–211.

[16] Marchio A, Meddeb M, Pineau P, Danglot G, Tiollais P, Bernheim A, Dejean A. Recurrent chromosomal abnormalities in hepatocellular carcinoma detected by comparative genomic hybridization. Genes Chromosomes Cancer 1997;18:59–65.

[17] Kusano N, Shiraishi K, Kubo K, Oga A, Okita K, Sasaki K. Genetic aberrations detected by comparative genomic hybridization in hepatocellular carcinomas: their relationship to clinicopathological features. Hepatology 1999;29:1858–62.

[18] Guan XY, Fang Y, Sham JS, Kwong DL, Zhang Y, Liang Q, Li H, Zhou H, Trent JM. Recurrent chromosome alterations in hepatocellular carcinoma detected by comparative genomic hybridization. Genes Chromosomes Cancer 2000;29:110–6.

[19] Poon TC, Wong N, Lai PB, Rattray M, Johnson PJ, Sung JJ. A tumor progression model for hepatocellular carcinoma: bioinformatic analysis of genomic data. Gastroenterology 2006;131:1262–70.

[20] Knuutila S, Björkqvist AM, Autio K, Tarkkanen M, Wolf M, Monni O, Szymanska J, Larramendy ML, Tapper J, Pere H, El-Rifai W, Hemmer S, Wasenius VM, Vidgren V, Zhu Y. DNA copy number amplifications in human neoplasms: review of comparative genomic hybridization studies. Am J Pathol 1998;152:1107–23.

[21] Larramendy ML, Virolainen M, Tukiainen E, Elomaa I, Knuutila S. Chromosome band 1q21 is recurrently gained in desmoid tumors. Genes Chromosomes Cancer 1998;23:183–6.

[22] Dor I, Namba M, Sato J. Establishment and some biological characteristics of human hepatoma cell lines. Gann 1975;66:385–92.

[23] Alexander JJ, Bey EM, Geddes EW, Lecatsas G. Establishment of a continuously growing cell line from primary carcinoma of the liver. S Afr Med J 1976;50:2124–8.

[24] Hirohashi S, Shimosato Y, Kameya T, Koide T, Mukojima T, Taguchi Y, Kageyama K. Production of alpha-fetoprotein and normal serum proteins by xenotransplanted human hepatomas in relation to their growth and morphology. Cancer Res 1979;39:1819–28.

[25] Nakabayashi H, Taketa K, Miyano K, Yamane T, Sato J. Growth of human hepatoma cells lines with differentiated functions in chemically defined medium. Cancer Res 1982;42:3858–63.
[26] Aden DP, Fogel A, Plotkin S, Damjanov I, Knowles BB. Controlled synthesis of HBsAg in a differentiated human liver carcinoma-derived cell line. Nature 1979;282:615–6.
[27] Park JG, Lee JH, Kang MS, Park KJ, Jeon YM, Lee HJ, Kwon HS, Park HS, Yeo KS, Lee KU. Characterization of cell lines established from human hepatocellular carcinoma. Int J Cancer 1995;62:276–82.
[28] Fujise K, Nagamori S, Hasumura S, Homma S, Sujino H, Matsuura T, Shimizu K, Niiya M, Kameda H, Fujita K. Integration of hepatitis B virus DNA into cells of six established human hepatocellular carcinoma cell lines. Hepatogastroenterology 1990;37:457–60.
[29] Huh N, Utakoji T. Production of HBs-antigen by two new human hepatoma cell lines and its enhancement by dexamethasone. Gann 1981;72:178–9.
[30] Kennedy GC, Matsuzaki H, Dong S, Liu WM, Huang J, Liu G, Su X, Cao M, Chen W, Zhang J, Liu W, Yang G, Di X, Ryder T, He Z, Surti U, Phillips MS, Boyce-Jacino MT, Fodor SP, Jones KW. Large-scale genotyping of complex DNA. Nat Biotechnol 2003;21:1233–7.
[31] Di X, Matsuzaki H, Webster TA, Hubbell E, Liu G, Dong S, Bartell D, Huang J, Chiles R, Yang G, Shen MM, Kulp D, Kennedy GC, Mei R, Jones KW, Cawley S. Dynamic model based algorithms for screening and genotyping over 100 K SNPs on oligonucleotide microarrays. Bioinformatics 2005;21:1958–63.
[32] Huang J, Wei W, Zhang J, Liu G, Bignell GR, Stratton MR, Futreal PA, Wooster R, Jones KW, Shapero MH. Whole genome DNA copy number changes identified by high density oligonucleotide arrays. Hum Genomics 2004;1:287–99.
[33] Minamiya Y, Matsuzaki I, Sageshima M, Saito H, Taguchi K, Nakagawa T, Ogawa J. Expression of tissue factor mRNA and invasion of blood vessels by tumor cells in non-small cell lung cancer. Surg Today 2004;34:1–5.
[34] Klemsz M, Hromas R, Raskind W, Bruno E, Hoffman R. PE-1, a novel ETS oncogene family member, localizes to chromosome 1q21-q23. Genomics 1994;20:291–4.
[35] Denda-Nagai K, Irimura T. MUC1 in carcinoma-host interactions. Glycoconj J 2000;17:649–58.
[36] Bongarzone I, Pierotti MA, Monzini N, Mondellini P, Manenti G, Donghi R, Pilotti S, Grieco M, Santoro M, Fusco A. High frequency of activation of tyrosine kinase oncogenes in human papillary thyroid carcinoma. Oncogene 1989;4:1457–62.
[37] Midorikawa Y, Tsutsumi S, Nishimura K, Kamimura N, Kano M, Sakamoto H, Makuuchi M, Aburatani H. Distinct chromosomal bias of gene expression signatures in the progression of hepatocellular carcinoma. Cancer Res 2004;64:7263–70.
[38] Qi H, Fillion C, Labrie Y, Grenier J, Fournier A, Berger L, El-Alfy M, Labrie C. AlbZIP, a novel bZIP gene located on chromosome 1q21.3 that is highly expressed in prostate tumors and of which the expression is upregulated by androgens in LNCaP human prostate cancer cells. Cancer Res 2002;62:721–33.
[39] Baillat D, Hakimi MA, Naar AM, Shilatifard A, Cooch N, Shiekhattar R. Integrator, a multiprotein mediator of small nuclear RNA processing, associates with the C-terminal repeat of RNA polymerase II. Cell 2005;123:265–76.
[40] Ilardi JM, Mochida S, Sheng ZH. Snapin: a SNARE-associated protein implicated in synaptic transmission. Nat Neurosci 1999;2:119–24.
[41] Starcevic M, Dell'Angelica EC. Identification of snapin and three novel proteins (BLOS1, BLOS2, and BLOS3/reduced pigmentation) as subunits of biogenesis of lysosome-related organelles complex-1 (BLOC-1). J Biol Chem 2004;279:28393–401.

The strength of CEUS compared with CT and MRI is the ability to assess the pattern of vascularity in real time, which can accurately characterize certain liver lesions. This has been illustrated by Wang *et al.*[4] in this issue of the Journal, confirming that this is a technique which can be used in routine clinical practice. Some benign lesions have characteristic patterns of enhancement which are diagnostic. Peripheral, nodular enhancement which progresses centripetally is diagnostic for a hemangioma. Focal nodular hyperplasia has centrifugal enhancement with a central feeding artery which tends to branch in a radial 'spoke-wheel' pattern. Malignant lesions show a dysmorphic pattern of vascular enhancement. Primary HCC classically has arterial phase enhancement, progressing rapidly to diffuse filling due to hepatic arterial supply, whereas metastatic lesions classically demonstrate rim or sparse central enhancement.[5]

The European Federation of Societies for Ultrasound in Medicine and Biology (EFSUMB)[14] has provided a series of guidelines which describe the areas where CEUS of the liver can have a clear-cut clinical impact. These include:

1 Characterization of focal lesions incidentally detected in patients with no known chronic liver disease.
2 Characterization of focal lesions in surveillance programs of chronic liver disease.
3 Staging and follow up of cancer patients.
4 Focal lesions with inconclusive MRI/CT or cytology/histology results.
5 Characterization of portal vein thrombosis.

In conclusion, the article by Wang *et al.* further supports the evidence that contrast enhanced ultrasound is a safe imaging modality which has the ability to characterize indeterminate liver lesions in real time. The advantage of immediately characterizing a lesion detected on unenhanced ultrasound is potentially time and cost saving because further investigations can be averted. This may also avoid unnecessary patient anxiety. CEUS also provides an option where CT or MR imaging is either contraindicated or yields equivocal findings. As with any new modality, there is a learning curve, and there is also the issue of the relative 'operator dependence' of ultrasound. Nevertheless, with increasing experience with the use of CEUS in more centers there is no doubt that CEUS will gain increasing value in routine clinical practice for the evaluation of focal liver lesions.

References

1 Bolondi L, Correas JM, Lencioni R, Weskott HP, Piscaglia F. New perspectives for the use of contrast-enhanced liver ultrasound in clinical practice. *Dig. Liver Dis.* 2007; **39**: 187–95.
2 Leen E, Ceccotti P, Kalogeropoulou C, Angerson WJ, Moug SJ, Horgan PG. Prospective multicenter trial evaluating a novel method of characterizing focal liver lesions using contrast-enhanced sonography. *AJR* 2006; **186**: 1511–9.
3 Wilson SR, Jang HJ, Kim TK, Burns PN. Diagnosis of focal liver masses on ultrasonography: comparison of unenhanced and contrast-enhanced scans. *J. Ultrasound Med.* 2007; **26**: 775–87.
4 Wang ZL, Tang J, Weskott HP *et al.* Undetermined focal liver lesions in gray scale ultrasound in patients with fatty liver: characterization with contrast-enhanced ultrasound. *J. Gastroenterol. Hepatol.* 2008; **23**: 1511–9.
5 Abraham JL, Thakral C. Tissue distribution and kinetics of gadolinium and nephrogenic systemic fibrosis. *Eur. J. Radiol.* 2008; **66**: 200–7.
6 Burns PN, Wilson SR. Focal liver masses: enhancement patterns on contrast-enhanced images—concordance of US scans with CT scans and MR images. *Radiology* 2007; **242**: 162–74.
7 Burns PN, Wilson SR. Microbubble contrast for radiological imaging: 1. *Principles. Ultrasound Q.* 2006; **22**: 5–13.
8 Bartolotta TV, Taibbi A, Midiri M, Lagalla R. Focal liver lesions: contrast-enhanced ultrasound. *Abdom. Imaging* 2008; [DOI: 10.1007/s00261-008-9378-6.
9 Wilson SR, Burns PN. An algorithm for the diagnosis of focal liver masses using microbubble contrast-enhanced pulse-inversion sonography. *AJR Am. J. Roentgenol.* 2006; **186**: 1401–12.
10 Jang HJ, Kim TK, Wilson SR. Imaging of malignant liver masses: characterization and detection. *Ultrasound Q.* 2006; **22**: 19–29.
11 Nicolau C, Catalá V, Vilana R *et al.* Evaluation of hepatocellular carcinoma using SonoVue, a second generation ultrasound contrast agent: correlation with cellular differentiation. *Eur. Radiol.* 2004; **14**: 1092–9.
12 Jang HJ, Kim TK, Burns PN, Wilson SR. Enhancement patterns of hepatocellular carcinoma at contrast-enhanced US: comparison with histologic differentiation. *Radiology* 2007; **244**: 898–906.
13 Fan ZH, Chen MH, Dai Y *et al.* Evaluation of primary malignancies of the liver using contrast-enhanced sonography: correlation with pathology. *AJR Am. J. Roentgenol.* 2006; **186**: 1512–19.
14 Claudon M, Cosgrove D, Albrecht T *et al.* Guidelines and good clinical practice recommendations for contrast enhanced ultrasound (CEUS)—update 2008. *Ultraschall Med.* 2008; **29**: 28–44.

Optimal imaging of hepatic mass lesions

Osamu Matsui, Toshifumi Gabata and Satoshi Kobayashi

Department of Radiology, Kanazawa University Graduate School of Medical Science, Kanazawa, Japan

See article in *J. Gastroenterol. Hepatol.* 2008; 23: 1465–1466 and 1520–1527.

There are many valuable imaging modalities for imaging a diagnosis of hepatic mass lesions. These include ultrasound (with and without contrast enhancement [CEUS]), computed tomography (CT), magnetic resonance imaging (MRI), nuclear medicine, angiography, combined CT and angiography, and positron emission tomography (PET). Each of these has unique capabilities, advantages and shortcomings, and can present information different from the other imaging modalities. None is completely superior to the others and, usually, diagnosis is made possible by the combination of several types of imaging methods. In addition, the availability and costs of these modalities are remarkably different between different countries or regions. Therefore, how to select the

Accepted for publication 7 July 2008.

Correspondence
Professor Osamu Matsui, Department of Radiology, Kanazawa University Graduate School of Medical Science, 13-1 Takara-machi, Kanazawa 920-8641, Japan. Email: matsuio@med.kanazawa-u.ac.jp

most suitable imaging method in the particular clinical setting has been challenging until now. Many scientific, clinical and economical comparative studies have been carried out without definite conclusion.

When availability and economic problems in each region are not considered, we can propose relatively acceptable algorithms for selection of imaging modalities for the diagnosis of hepatic mass lesions from the scientific point of view. In this Editorial, we would like to propose the optimal imaging for common hepatic mass lesions using contemporary and widely commercially available imaging modalities including multi-row detector CT (MDCT) with 64 detectors, 3T MRI, and PET. Here, we will base our recommendations according to recently reported scientific analyses and our personal clinical experience.

For the detection of hepatic mass lesions, ultrasound is the first choice because of its high diagnostic accuracy with less invasiveness, less harm, easy availability and easy portability. Hepatic mass lesions larger than 1.5 cm in diameter can be commonly detected by conventional ultrasound using up-to-date equipment. Use of contrast agents which accumulate in the hepatic reticuloendothelial system for ultrasonography (CEUS) facilitates identification of lesions as small as approximately 0.5 cm diameter during the delayed parenchymal phase;[1,2] developments in CEUS are discussed in another Editorial in this issue of the *Journal of Gastroenterology and Hepatology*.[3] This is almost comparable to that in superparamagnetic iron oxide particles (SPIO) or hepatobiliary contrast-enhanced MRI, which is now considered to be the most accurate non-invasive method for the detection of hepatic mass lesions.[4–8] For the detection of hypervascular mass lesions, dynamic CT using MDCT and dynamic MRI are sensitive and lesions down to approximately 0.5 cm in diameter can be detected. Therefore, for the detection (screening) of hypervascular cancers, such as hepatocellular carcinoma (HCC), the combination of ultrasound and dynamic CT or MRI is now commonly carried out in endemic areas. However, if other technologies become more readily available, CEUS or MRI with SPIO or hepatobiliary contrast may become the first-line procedure for the detection of hepatic mass lesions in the near future.[8]

However, for the detection of early HCC with highly well-differentiated cancer cells with internal Kupffer cells and hepatobiliary function, some problems remain. This is because these contrast agents have shown variable degrees of accumulation in this type of early-stage HCC.[4] Therefore, conventional ultrasound may continue to be an important screening procedure for HCC in high-risk patient groups. CT during arterial portography (CTAP) and CT during hepatic arteriography are invasive because of catheter insertion into the hepatic or superior mesenteric artery. However, it is still widely carried out as a preoperative (or pretreatment) final staging modality, especially in Japan.[9]

For the precise characterization of hepatic mass lesions, we should know the features of each imaging modality and select the most suitable method according to each clinical setting. The definite diagnosis of a simple hepatic cyst can be made possible by ultrasound, CT and MRI and, usually, ultrasound with no further examination is sufficient. For the characterization of solid mass lesions, visualization of macroscopic features of the lesions, determination or estimation of the internal tissue components such as necrosis, fat, hemorrhage, iron, mucin, fibrous tissue, vascularity (blood supply), and the function of internal cells or tissues are useful. For the visualization of the internal macroscopic pathology of a lesion, ultrasound and MRI may be most valuable, whereas for hypervascular lesions, dynamic study by contrast agent using ultrasound, CT and MRI often well visualize them, as has been well known for the depiction of mosaic and capsular architecture in moderately differentiated, typical HCC. Configuration of the lesion is most precisely demonstrated by reticuloendothelial specific contrast ultrasound and SPIO or hepatobiliary contrast-enhanced MRI. Internal necrosis is definitely diagnosed by dynamic study with contrast agent on ultrasound, CT and MRI because of the lack of tissue perfusion. The existence of fat, hemorrhage and iron can be made possible by CT and MRI more specifically and precisely by the latter. Estimation of internal fibrous tissue is also valuable for the differential diagnosis of hepatic solid mass lesions. This commonly shows delayed enhancement on equilibrium (or delayed) phase of dynamic CT or MRI, without definite enhancement on the arterial dominant phase, and is also depicted with greater sensitivity on MRI. Evaluation of vascularity or blood supply is possible only by imaging such as Doppler ultrasound, CEUS and dynamic CT and MRI. All these modalities visualize vascularity well, but the most sensitive methods in each lesion are CEUS and dynamic MRI. In contrast, for the evaluation of multiple lesions, dynamic CT using MDCT has great value because of its high spatial resolution and objectivity for transmission of the information obtained to clinicians. On particular occasions, in Japan, such as for the characterization of early HCC, CT during arterioportography (CTAP) and CT during hepatic arteriography are carried out to evaluate the arterial supply and portal supply separately.[10,11]

When reticuloendothelial or hepatobiliary function is shown in the lesion, this usually indicates its hepatocellular origin. This is very important for differential diagnosis and, for this purpose, CEUS and MRI with tissue-specific contrast agents are valuable. However, it has been well verified that early-stage well-differentiated HCC very often have these functions, and care should therefore be taken in differential diagnosis from other benign hepatocellular nodules, such as focal nodular hyperplasia. The diagnostic value of PET for hepatic mass lesion is not appreciable and PET is therefore carried out only for the evaluation of extrahepatic spread of malignant hepatic tumors, such as cholangiocarcinoma.

As expected from the above description, it is not easy to simply delineate a single algorithm for the optimal imaging of hepatic mass lesions. From a scientific point of view, ultrasound including CEUS may be the first-choice modality because of the reasons mentioned above and those which are also discussed in the accompanying Editorial.[3] The second-line procedure may be MRI, including dynamic study, as Balci *et al.* report in this issue of the Journal.[12] This is suggested because dynamic MRI confers a wide-ranging ability to visualize the pathology of mass lesions, as well as high contrast resolution in contrast studies. In addition, the information provided by MRI with liver tissue-specific contrast agents cannot be demonstrated by other imaging methods; the resultant ability to detect and characterize hepatic mass lesions is extremely high. Therefore, when no technical problems are encountered during scanning, the combination of ultrasound and MRI with contrast studies conveys the capability to resolve almost all diagnostic problems. Finally, when some problems are encountered with definitive MRI examination, CT and arteriographic procedures may

be indicated. It is also noted that no radiation is involved with MRI, in contrast to CT and angiographic procedures.

In spite of the scientific superiority of MRI, in reality, it is still impossible to carry out the most modern MRI procedures in many countries, especially some of those where HCC is endemic. Japan has the largest number of MRI machines per population in the world. However, it is still not always possible to perform MRI (instead of CT) as the second-line procedure for the diagnosis of hepatic lesions because of logistical constraints. MRI is now the first and inevitable diagnostic procedure for central nervous system, bone and soft tissue diseases, and genitourinary diseases and, for this reason, MRI services are always busy in all hospitals. In addition, MRI is still too expensive to cover all patients in many countries, including Japan. Because of these reasons, CT is now, and may remain so during the coming 10 years, the second-line procedure for the diagnosis of hepatic mass lesions in many countries or regions.

References

1 Kudo M. New sonographic techniques for the diagnosis and treatment of hepatocellular carcinoma. *Hepatol. Res.* 2007; **37** (Suppl 2): S193–9.
2 Nakano H, Ishida Y, Hatakeyama T *et al.* Contrast-enhanced intraoperative ultrasonography equipped with late Kupffer-phase image obtained by sonazoid in patients with colorectal liver metastases. *World J. Gastroenterol.* 2008; **28**: 3207–11.
3 Ong Y, Gibson RN. Contrast-enhanced ultrasound: Emerging modality for liver lesion characterization. *J. Gastroenterol. Hepatol.* 2008; **23**: 1465–6.
4 Tanimoto A, Wakabayashi G, Shinmoto H, Nakatsuka S, Okuda S, Kuribayashi S. Superparamagnetic iron oxide-enhanced MR imaging for focal hepatic lesions: a comparison with CT during arterioportography plus CT during hepatic arteriography. *J. Gastroenterol.* 2005; **40**: 371–80.
5 Imai Y, Murakami T, Yoshida S *et al.* Superparamagnetic iron oxide-enhanced magnetic resonance images of hepatocellular carcinoma: correlation with histological grading. *Hepatology* 2000; **32**: 205–12.
6 Rappeport ED, Loft A, Berthelsen AK *et al.* Contrast-enhanced FDG-PET/CT vs. SPIO-enhanced MRI vs. FDG-PET vs. CT in patients with liver metastases from colorectal cancer: a prospective study with intraoperative confirmation. *Acta Radiol.* 2007; **48**: 369–78.
7 Choi JY, Kim MJ, Kim JH *et al.* Detection of hepatic metastasis: manganese- and ferucarbotran-enhanced MR imaging. *Eur. J. Radiol.* 2006; **60**: 84–90.
8 Hammerstingl R, Huppertz A, Breuer J *et al.* Diagnostic efficacy of gadoxetic acid (Primovist)-enhanced MRI and spiral CT for a therapeutic strategy: comparison with intraoperative and histopathologic findings in focal liver lesions. *Eur. Radiol.* 2008; **18**: 457–67.
9 Nomura K, Kadoya M, Ueda K, Fujinaga Y, Miwa S, Miyagawa S. Detection of hepatic metastases from colorectal carcinoma: comparison of histopathologic features of anatomically resected liver with results of preoperative imaging. *J. Clin. Gastroenterol.* 2007; **41**: 789–95.
10 Hayashi M, Matsui O, Ueda K *et al.* Correlation between the blood supply and grade of malignancy of hepatocellular nodules associated with liver cirrhosis: evaluation by CT during intraarterial injection of contrast medium. *AJR Am. J. Roentgenol.* 1999; **172**: 969–76.
11 Ueda K, Matsui O, Kawamori Y *et al.* Hypervascular hepatocellular carcinoma; evaluation of hemodynamics with dynamic CT during hepatic arteriography. *Radiology* 1998; **206**: 161–6.
12 Balci NC, Befeler AS, Leiva P, Pilgram TK, Havlioglu N. Imaging of liver disease: Comparison between quadruple phase multidetector computed tomography and magnetic resonance imaging. *J. Gastroenterol. Hepatol.* 2008; **23**: 1520–7.

Intraductal ultrasound in biliary disorders

Tiing Leong Ang and Kwong Ming Fock

Division of Gastroenterology, Department of Medicine, Changi General Hospital, Singapore

See article in *J. Gastroenterol. Hepatol.* 2008; 23: 1590–1595.

Transabdominal ultrasound (US), computed tomography (CT), magnetic resonance cholangiopancreatography (MRCP), endoscopic ultrasound (EUS) and endoscopic retrograde cholangiopancreatography (ERCP) are imaging modalities commonly used in the evaluation of biliary disorders. The use of intraductal ultrasound (IDUS) to investigate biliary disorders was first published in 1992[1,2] but utilization and knowledge of its usefulness remains low in clinical practice. In the light of the study by Tsuchiya *et al.* that assessed the value of IDUS in decreasing the rate of recurrent biliary stones after endoscopic papillotomy (EPT) in this issue of the *Journal of Gastroenterology and Hepatology*,[3] it is timely to review the clinical utility of IDUS.

IDUS is carried out during ERCP by inserting a catheter probe over a guidewire into the bile duct.[4] Real-time cross-sectional ultrasonic examination of the bile duct wall and its contents is performed by slowly withdrawing the probe. Because the ultrasonic tip is in close proximity to the biliary tree, high-resolution cross-sectional images of the wall and contents of the biliary tree can be obtained. Indeed, IDUS has proven be to very useful in the evaluation of biliary strictures, in staging cholangiocarcinoma and in the diagnosis of bile duct stones. In particular, as shown by Tsuchiya *et al.*,[3] IDUS is especially useful for detecting small bile duct stones that may be missed during the initial cholangiogram, or that may persist after stone extraction. Upon detection of such small stones, further endoscopic interventions and stone extraction can then be carried out, thus preventing recurrent biliary events.

IDUS is useful in differentiating benign and malignant biliary strictures. The IDUS image of a normal bile duct consists of usually two or, sometimes, three sonographic layers. When visualized as a two-layer structure, the internal hypoechoic layer comprises the mucosa, muscularis propria and fibrous layer of the subserosa, while the outer hyperechoic layer reflects the adipose layer of the subserosa, the serosa and the interface echo between the serosa and surrounding organs. There may occasionally be a third inner hyper-

Accepted for publication 4 July 2008.

Correspondence
Professor Kwong Ming Fock, Division of Gastroenterology, Department of Medicine, Changi General Hospital, 2 Simei Street 3, Singapore 529889. Email: kwong_ming_fock@cgh.com.sg